Design Considerations for a Heterogeneous Network of Bearings-only Sensors using Sensor Management

Lance M. Kaplan
U.S. Army Research Laboratory
Adelphi, MD 20783

Volkan Cevher
University of Maryland
College Park, MD 20742

Abstract— This paper presents the design characterization of a heterogeneous sensor network with the goal of geolocation accuracy. It is assumed that the network exploits sensor management to conserve node usage. Each available node modality is a bearings-only sensor of varying capability. The optimal mixture of modalities is discussed under the constraint of the overall network cost. Finally, simulations verify the theory and demonstrate design choices for a network consisting of two modes analogous to acoustic arrays and cameras.

Keywords— Sensor networks, sensor fusion, Poisson point process

TABLE OF CONTENTS

1. INTRODUCTION

The paradigm of the network of inexpensive sensors distributed geographically over a large region promises to provide improved surveillance capabilities for a number of applications [1]. Each sensor node on its own consists of the sensor to collect measurements, a radio to share data with other nodes, a microprocessor to process and fuse data into information and a battery to provide the necessary power for the hardware to work. Alone, a sensor node is only able to gain limited inference about objects of interest, i.e., targets, in the surveillance region. By sharing data over the sensor network, each node is able to gain much better inference about the scene. In many applications, the sensor network must operate in a clandestine manner where the nodes are dispersed via airdrop or cannon fire. Therefore, the physical size of each node is limited, and it is impossible to maintain the nodes and replenish batteries. Therefore, the nodes must operate under severe energy constraints to maintain a long effective lifetime [2].

In the sensor network research literature, the network management problems concern themselves for developing strategies to self-organize a set of available sensors for optimal resource allocation, e.g., [3], [4], [5], [6], [7], [8]. The solution of this problem is quite important because the effective lifetime of an already deployed sensor network can be increased by saving sensor batteries via using clever schemes of sensor selection, information hand-off, and efficient data compression. In [9], we investigate an optimal resource allocation problem on randomly deployed sensor networks for position tracking. Our focus is the the network build strategy (NBS), which determines the number of sensors of different types to deploy from a sensor pool that offers a distinct cost vs. performance trade-off for each type of sensor. We formulate the NBS problem as a constrained optimization problem, whose objective is to minimize the position uncertainty under a limited budget by determining a build strategy. Hence, the results of the NBS problem is complimentary to the sensor network management literature that concentrates on a choice of a subset of already deployed sensors in the field to maximize battery life while simultaneously minimizing the location uncertainty.

In this paper, using similar assumptions to [9], we focus on the design of a random heterogeneous sensor network when only a constant number of sensors are used for position estimation. This is a practical situation because it is proven that a small subset of sensors is always competitive with the full network in localization performance [10]. We assume that there are T possible sensor types, i.e. modalities. For this paper, it is assumed that all sensor types collect target bearing measurements within the ground plane, i.e., azimuth angle to the target. The difference among modalities is the field of view (FOV), accuracy, environmental robustness and monetary cost of the sensors. When the FOV is limited (less than 360°), the sensor will only be able to see the target and collect a bering measurement when the target moves within the line-of-sight of the sensor. Because of energy limitations, a sensor node has no capability to pan and tilt in order change its orientation to bring a target within line-of-sight. The accuracy of the sensor is related to the expected error between the measured bearing and actual bearing. A sensor may not be able to collect useful measurements during certain environmental conditions; thus, it may lack environmental robustness. Finally, there is always a budget for the network, and the cheaper a sensor type, the more nodes that one can include

1-4244-0525-4/07/$20.00/©2007 IEEE.
IEEEAC paper #1687, Version 3, Updated Dec 1, 2006

in the network.

The design goal for this paper is to optimize the geolocation performance of the randomly deployed sensor network for any point well inside the deployment region. The design choices are the number of senors that comprise each type. The design constraint is the overall cost of all the nodes comprising the network. The geolocation performance is based on the fact that while the network is tracking targets, it is using sensor management to control the node usage. The sensor management approaches use the predicted target/node geometry to determine the best subset of nodes in terms of expected geolocation accuracy [3], [4], [11], [5], [6], [7], [8]. As shown in [4], it is possible to implement the node selection over a decentralized architecture [12]. In general, the analysis of geolocation performance with sensor management can become unruly. For the analysis to be tractable, this paper considers a simplified management technique: selection of the two normalized closest nodes to the target. The normalization is based upon the accuracy of the modality of the particular node.

The paper presents theory applicable to an arbitrary number T of sensor types and includes simulations that focus on two sensor types that serve as analogs to acoustic arrays and cameras. The acoustic arrays are robust omni-directional senors, while the cameras are more accurate but also more expensive and less environmentally robust. For instance, under foggy conditions, one can still use the microphones but not the cameras. The simulations consists of generating random configurations of sensor networks and Monte Carlo evaluation of extended Kalman filter (EKF) trackers. The simulations verify when the theory is accurate and show how to determine the number of sensors for each modality given the overall network budget.

The paper is organized as follows. Section 2 discusses the sensor model parameters. Then, Section 3 reviews the Cramer-Rao lower bound (CRLB) for bearings-only target localization, sensor selection and the statistics for the node locations relative to the target. This review provides the background which is used in Section 4 to present a new theory to characterize localization performance as a function of the design parameters. Section 4 also discusses the general optimization problem to determine the best design parameters. Then, simulations are provided in Section 5 to validate the theory and to illustrate good design choices for sensor networks. Finally, Section 6 provides concluding remarks and discussions of future directions of research.

2. SENSOR MODELS

The paper makes a number of simplifying assumptions so that the analysis is tractable. First, it is assumed that calibration and synchronization issues can be ignored. Nodes may have limited FOV and lack the ability to change their orientation to obtain a better view of the target. Next, each node always detects the target, if it lies within the FOV of the node, and never detects a false target. When a node detects the target, it provides a bearing measurement where the error follows an additive white Gaussian noise (AWGN) model. The nodes are always working, but conditions may exist where the some nodes are unable to provide meaningful measurements. The wireless communication channels between nodes are always operating perfectly. Using these assumptions, this section explains the salient parameters that describe the sensing behavior of any node. The section wraps up by describing parameters that could serve as analogs for acoustic arrays and cameras.

Generic Model

At a given snapshot of time, the sensor node collects a bearing measurement that is representative of the current bearing ϕ between the node and the target. More precisely, the measurement is a noisy version of the retarded bearing ϕ^*, where retarded bearing refers to the fact that there is a propagation delay between the time the target emits the signal that the node is measuring. Therefore, the node is actually collecting data consistent with a bearing from a retarded time. Thus, the bearing measurement AWGN model is

$$\tilde{\phi} = \phi^* + \eta, \tag{1}$$

where $\eta \sim N(0, \sigma^2)$, ϕ^* is the retarded bearing, and σ is the bearing root mean squared (RMS) error. The RMS bearing error σ represents the measurement accuracy of the node, and this value impacts the localization accuracy of integrating measurements from multiple nodes.

If the target is not moving, ϕ^* corresponds to the bearing to the target at the current time, i.e., $\phi^* = \phi$. For a constant velocity target [13],

$$\phi^* = \phi + \arcsin\left(\frac{v}{c}\sin(\phi - \psi)\right), \tag{2}$$

where v and ψ is the speed and heading of the target, respectively, and c is the propagation speed of the signal being measured. The tracking simulations take into account the propagation delay using (2). However, the error analysis for the sensor networks assumes that $\phi^* = \phi$ in the AWGN model given in (1).

The sensor is fixed on the ground with an orientation of φ. The normalized FOV of the sensor is α where $0 < \alpha \leq 1$. This means that the sensor is able to see a target and report a bearing measurement if

$$\frac{|\phi^* - \varphi|}{\pi} \leq \alpha. \tag{3}$$

If $\alpha = 1$, the sensor is omni-directional and always reports a measurement. The FOV in units of degrees is $360^\circ\alpha$.

The environmental conditions may prevent the sensors from collecting useful measurements. This phenomena is modeled by the operational probability p_{op}. Therefore, there is a probability of $1 - p_{\text{op}}$ that the sensor is can not be operational.

The final parameter is the unit cost of the sensor. We let ζ represent the cost of the sensor. The cost of the sensor constrains how many nodes of a particular modality can be employed in the sensor network.

Acoustic Arrays

An array of microphones can determine the target bearing by considering the time delays, i.e., phase differences, between the microphone. Because target typically emit harmonics, it is advantageous to apply a wideband direction of arrival (DOA) algorithm, e.g., [14], [15]. As shown in [13], σ is in the order of 3 to 4 degrees. Therefore, we model acoustic arrays with $\sigma = 5^\circ$. The simulations take into account the time retardation factor given by (2) by setting the speed of sound as $c \approx 347$ m/s. Furthermore, the circular arrays are omnidirectional so that $\alpha = 1$. Finally, we suspect that the acoustic arrays will always provide useful measurements when the cameras can see the targets. Therefore, $p_{\text{op}} = 1$. Finally, the unit cost of the acoustic array is normalized to a value of one monetary units, i.e., $\zeta = 1$.

Cameras

Cameras determine the bearing by detecting which pixel includes the target. The size of the pixels, i.e., instantaneous FOV (IFOV), is determined by the FOV divided by the number of pixels comprising the length and width of the imagery. The FOV varies depending on the design of the optics. We consider two values for the FOV: $\alpha = \frac{1}{12}$ (30°) and $\alpha = \frac{1}{3}$ (120°). We assume that bearing error is in the order of twice the IFOV. By considering that the narrow FOV camera contains about 240 pixels per dimension, then a reasonable value of for the bearing error is $\sigma = 0.25^\circ$. We assume that the wider FOV camera contains more pixels to maintain this value of σ. The simulations ignore the time retardation factor in (2) because the speed of light is so large. There are conditions when the cameras can not collect measurements, but the microphones can, e.g., foggy weather. Therefore, it reasonable for $p_{\text{op}} < 1$. This paper analyzes the effect of different values of $p_{\text{op}} < 1$. Finally, we assume in this paper that cameras are ten times more expensive than microphones, i.e., $\zeta = 10$ monetary units.

3. SENSOR NETWORK THEORY

The section provides the background theory to develop the performance characterization for the sensor network design. The network consists of N sensors distributed uniformly over a large 2-D region on the ground of area A so that the sensor density is

$$\lambda = \frac{N}{A}. \tag{4}$$

The network is tracking a target that is well inside the physical boundaries of the network. Without loss of generality, the target is located at the origin of the coordinate system, and the nodes are indexed in ascending distance to the target. The polar coordinates for the nodes are labeled as (r_i, ϕ_i) for $i = 1, \ldots, N$, where r_i and ϕ_i are the distance and bearing between the target and the i-th node. Note that $0 \leq r_1 \leq r_2 \leq \ldots \leq r_N$. Finally, the bearing RMS error for the i-th node is σ_i. In this paper, the magnitude of σ_i is dictated by the corresponding sensor type for the i-th node.

Localization

Localization refers to the collection of bearings-only measurements over multiple nodes to estimate the position of the target. For any unbiased localization estimator, it is well known that the mean squared error (MSE) is bounded below by the Cramer-Rao lower bound (CRLB) [16]. This bound is derived from the Fisher information matrix (FIM). For the localization estimator using bearings-only measurements, the FIM is [17]

$$\mathbf{J} = \sum_{i \in \mathcal{N}_a} \frac{1}{\sigma_i^2 r_i^2} \begin{bmatrix} \sin^2 \phi_i & -\sin\phi_i \cos\phi_i \\ -\sin\phi_i \cos\phi_i & \cos^2 \phi_i \end{bmatrix}, \tag{5}$$

where $\mathcal{N}_a$ is the set of nodes that are actively collecting and sharing measurements for the given snapshot. Thus, the CRLB for the localization MSE is

$$\varepsilon(\mathcal{N}_a) = \text{trace}\left\{\mathbf{J}^{-1}\right\}, \tag{6}$$

$$= \frac{\text{trace}\left\{\mathbf{J}\right\}}{\det\left\{\mathbf{J}\right\}}, \tag{7}$$

where

$$\text{trace}\left\{\mathbf{J}\right\} = \sum_{i \in \mathcal{N}_a} \frac{1}{\sigma_i^2 r_i^2}, \tag{8}$$

and [3]

$$\det\{\mathbf{J}\} = \frac{1}{2} \sum_{i \in \mathcal{N}_a} \sum_{j \in \mathcal{N}_a} \frac{\sin^2(\phi_i - \phi_j)}{\sigma_i^2 r_i^2 \sigma_j^2 r_j^2}. \tag{9}$$

For the the CRLB to be finite, the active set $\mathcal{N}_a$ must contain two or more nodes with different bearings to the target. Otherwise, the determinant of the FIM given by (9) is zero. In tracking scenarios, it is possible for one node to be active at a time, i.e., $|\mathcal{N}_a| = 1$, because the current measurement is being integrated with measurements at previous times to form a full rank posteriori FIM [3].

The expression for the position error in (7) represents the geometrical dilution of precision (GDOP) measure used in [11] for node selection. As shown in [11], [17], [18], [19], [20], (7) is consistent with the expected MSE for the maximum likelihood single snapshot geolocation approach. In fact, the FIM also represents the inverse covariance update in the information form of the EKF tracker [3]. In short, (7) is representative of the actual errors of practical localization estimators. It is also convenient to consider the root mean squared (RMS) localization error

$$\rho(\mathcal{N}_a) = \sqrt{\varepsilon(\mathcal{N}_a)}. \tag{10}$$

The simulations will provide results in terms of the RMS error because the corresponding units are natural (in terms of length).

Normalized Closest Sensor Management

To conserve energy, the sensor manager determines which nodes will be active for a given snapshot. A good sensor manager should balance localization accuracy with energy requirements such as communications via the radios. The "normalized closest" sensor manager is a simple approach to select the active set $\mathcal{N}_a$ of N_a nodes with small localization MSE as given by (7). Actually, the calculation of the MSE requires one to already know the location of the target relative to the target. In practice, the sensor manager performs the node selection while tracking the target, and the predicted target state is used to estimate the polar coordinates for the nodes.

The "normalized closest" approach selects the N_a nodes corresponding to the smallest normalized distances to the target

$$\tilde{r}_i = \sigma_i r_i. \tag{11}$$

The justification for the selection approach is because the localization MSE is bounded below by [3]

$$\varepsilon(\mathcal{N}_a) \geq \frac{4}{\text{trace}\,\{\mathbf{J}\}}. \tag{12}$$

The lower bound can be achieved when the nodes essentially surround the target. For the case of two nodes, this means that the two lines of sight between the nodes and the target are orthogonal. The normalized closest approach assumes that the node/target geometry is favorable so that the MSE is near its lower bound. Then, maximization of the MSE entails the minimization of the trace of the FIM, which is accomplished by selecting the nodes with small normalized distances to the target.

While the bearing error σ_i varies by node, it is generally constant over node type. In this paper, the bearing error is fixed for given sensor model (see Section 2). For the sake of mathematical tractability, $N_a = 2$. Note that the MSE diverges to infinity for $N_a = 1$ since the determinant of the FIM is zero. From (7), (8) and (9) it can be shown that the MSE for the two normalized closest nodes is

$$\varepsilon(\mathcal{N}_a) = \frac{\tilde{r}_1^2 + \tilde{r}_2^2}{\sin^2(\phi_1 - \phi_2)}. \tag{13}$$

Network Geometry

Given that the sensors are uniformly distributed over the deployment region of area A, the locations of the sensors over any patch of area P inside this region such that $P \ll A$ approximates a 2-D Poisson point process with density λ [21]. For any point inside the 2-D Poisson point process, the squared ordered distances to that point have the same joint density as the arrival times of a Poisson process with intensity $\gamma = \pi\lambda$ [22]. In addition, the polar angles between the arbitrary and the ordered sensors are independent identically distributed (i.i.d.) with a uniform distribution over $[0, 2\pi)$. Therefore, a very good approximation to the ordered squared distances to the target, $s_i = r_i^2$ for $i = 1, \ldots, k$, when $k \ll N$ is

$$f(s_1, \ldots, s_k) = \begin{cases} (\pi\lambda)^k e^{-\pi\lambda s_k} & \text{for } s_k \geq \ldots \geq s_1 \geq 0, \\ 0 & \text{otherwise,} \end{cases} \tag{14}$$

and the polar angles ψ_i are approximately uniform. Furthermore, the marginal distribution for s_i is approximated by a Gamma distribution

$$f(s_i) = \begin{cases} \frac{(\pi\lambda)^i}{(i-1)!}(s_i)^{i-1} e^{-\pi\lambda s_i} & \text{for } s_i \geq 0, \\ 0 & \text{otherwise.} \end{cases} \tag{15}$$

Figure 1 compares the distribution of the ordered squared distances described by the Gamma distribution to empirically generated histograms. The histograms were created by realizing 1000 different configuration of $N = 100$ nodes uniformly distributed over a circular region of radius 100m and then sorting the squared distances to the center of the region. Clearly, when $i \ll N$, the histograms match up with the Gamma distributions. For the case of $i = 50$ and $i = 100$, the Gamma distributions are too heavy tailed to be represented by the histograms of s_i.

4. SENSOR NETWORK DESIGN CHARACTERIZATION

The sensor network design characterization refers to the relation of the median localization error as a function of the design parameters, i.e., the number of sensors N_t for types $t = 1, \cdots, T$. To derive the characterization, the first subsection focuses on the case of the homogeneous network. Then, the second subsection extends the results to the general heterogeneous case and discusses the optimization of the median error under the cost constraint.

Homogeneous Network

The sensor network consists of nodes of type t whose bearing RMS error is σ_t. The normalized FOV of the nodes is α_t. Given that N_t nodes are uniformly distributed over a region of area A, then the node density is given by $\mu_t = N_t/A$. Over any patch inside the deployment region of area P such that $P \ll A$, the nodes form an approximate 2-D Poisson point process. Furthermore, the orientation of the nodes are uniformly distributed over $[0, 2\pi)$. Thus, the probability that the target is within the FOV of any node, i.e., (3) is satisfied, is α_t as long as the target is well inside the deployment region. In other words, the set of nodes that can see the target are formed by retaining nodes from a 2-D Poisson point process of density $\lambda = \mu_t$ with probability α_t. As a result, the line-of-sight nodes also form a 2-D Poisson point process of density $\lambda = \mu_t\alpha_t$ [21].

The calculation of the distribution of the localization MSE with sensor management (see (13)) requires the joint distribution of the normalized squared distances and the polar angles. As stated earlier, the distances are statistically independent from the polar angles, and the polar angles are

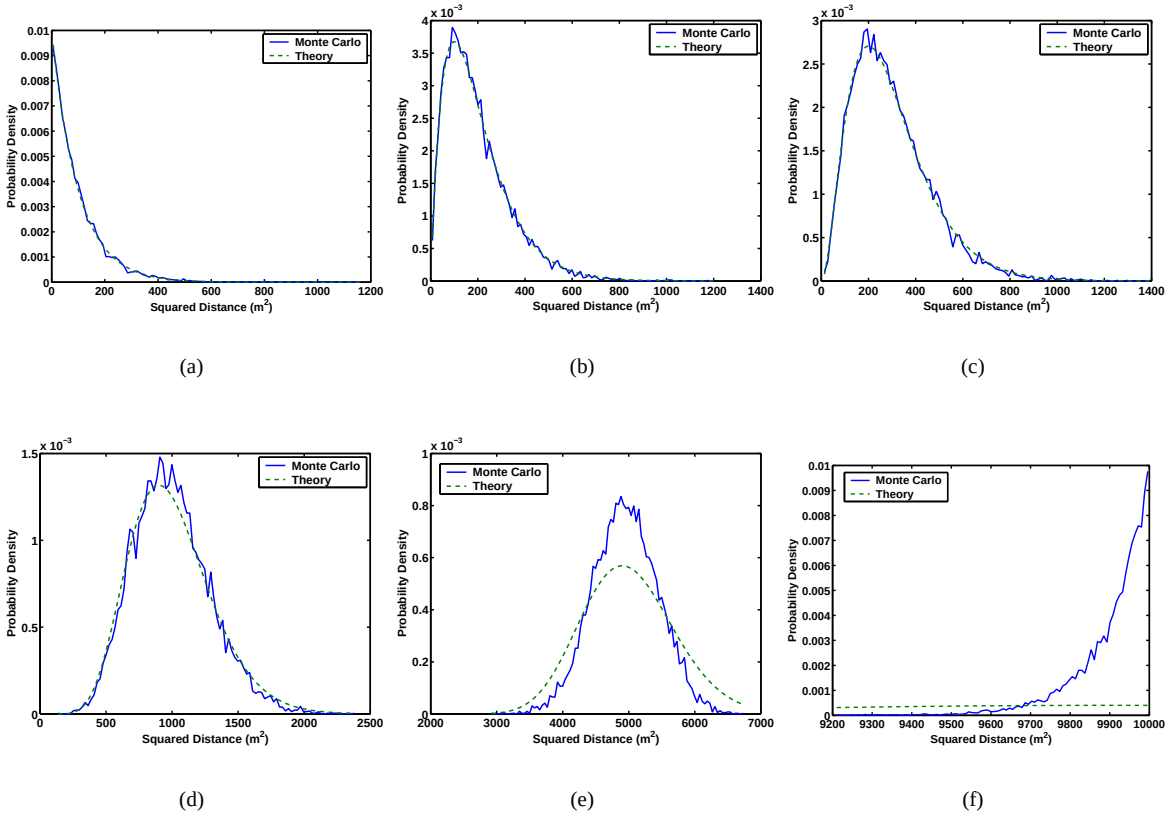

Figure 1. Comparison of Gamma distributions (theory) to empirical histograms (Monte Carlo) for the ordered squared distances to any arbitrary point inside a sensor network: (a) s_1, (b) s_2, (c) s_3, (d) s_{10}, (e) s_{50}, and (f) s_{100}.

i.i.d. with a uniform probability distribution function (pdf) over $[0, 2\pi)$. The joint distribution for the squared ordered distances is given by (14) where $\lambda = \mu_t \alpha_t$. The distribution for the squared ordered **normalized** distances is obtained by considering the following change of variables,

$$\tilde{s}_i = \tilde{r}_i^2, \quad (16)$$
$$= \sigma_t^2 s_i. \quad (17)$$

It can easily be shown that the joint distribution of $\tilde{s}_i$ is also given by (14), but now $\lambda = \frac{\mu_t \alpha_t}{\sigma_t^2}$. In the sequel, we refer to

$$\tilde{\mu}_t = \frac{\mu_t \alpha_t}{\sigma_t^2} \quad (18)$$

as the *normalized line-of-sight* density of the homogeneous network t, because, one can view the normalized squared distances as being generated from a Poisson point process of density $\tilde{\mu}_t$. Under the assumption that the sensors form a Poisson point process of density μ_t, the dilation of the line-of-sight sensors about the target by a factor of σ_t actually produces the Poisson point process of density $\tilde{\mu}_t$.

Now that the distribution of the components comprising the expression for localization MSE with sensor management is characterized, one can calculate the statistics for the localization MSE in (13). Unfortunately, as shown in Appendix A, the expected value of $\varepsilon(\mathcal{N}_a)$ or $\rho(\mathcal{N}_a)$ is not finite. This is due to the fact of the high likelihood that the two selected nodes will exhibit a poor geometry with respect to the target, i.e., comparable line-of-sight vectors to the target. Even though the high tail of the distribution of ε or ρ affects the calculation of a meaningful mean, one can still compute a finite median value. As shown in Appendix A, the cumulative distribution function (CDF) for the localization MSE is

$$F_\varepsilon(\varepsilon) = G(\tilde{\mu}_t \varepsilon), \quad (19)$$

where

$$G(x) = 1 - 2\beta\left(\frac{x}{2}\right) + \beta(x), \quad (20)$$

and

$$\beta(x) = \frac{1}{\pi}\int_0^\pi e^{-\pi x \sin^2\theta} d\theta. \quad (21)$$

The median value of ε is

$$\text{median}\{\varepsilon(\mathcal{N}_a)\} = \frac{G^{(-1)}(0.5)}{\tilde{\mu}_t}, \quad (22)$$
$$= G^{(-1)}(0.5)\frac{\sigma_t^2}{\mu_t \alpha_t}, \quad (23)$$

where $G^{(-1)}(\cdot)$ is the inverse function of $G(\cdot)$ and $G^{(-1)}(0.5) \approx 1.86$.

The CDF of localization RMS error ρ is simply determined by substituting (10) in the CDF for the localization MSE in (19),

$$F_\rho(\rho) = G(\tilde{\mu}_t \rho^2), \tag{24}$$

and the median of the RMS localization error is

$$\begin{aligned} \text{median}\{\rho(\mathcal{N}_a)\} &= \left(\frac{G^{(-1)}(0.5)}{\tilde{\mu}_t}\right)^{\frac{1}{2}}, & (25)\\ &\approx \frac{1.3639\sigma_t}{\sqrt{\mu_t \alpha_t}}. & (26) \end{aligned}$$

Heterogeneous Network

The network consists of T types of bearings-only sensor nodes covering a deployment region of area A. The RMS bearing error, normalized FOV and population for the t-th node type is σ_t, α_t, and N_t, respectively. At this point, we assume that all sensors types are operational under all conditions, i.e., $p_{\text{op},i} = 1$. When viewing the subnetwork of nodes consisting of only type t, the analysis of the previous subsection applies. That is each subnetwork can be viewed as a Poisson point process of density μ_t where the normalized target distances are dictated by the density $\tilde{\mu}_t$ given in (18). The heterogeneous network is simply the aggregate of the subnetworks formed by nodes of type t for $t = 1, \ldots, T$, and the additive property of Poisson process applies [21]. As a result, the normalized target distances are being generated from the normalized density

$$\begin{aligned} \tilde{\mu} &= \sum_{t=1}^{T} \tilde{\mu}_t, & (27)\\ &= \sum_{t=1}^{T} \frac{\mu_t \alpha_t}{\sigma_t^2}. & (28) \end{aligned}$$

When all sensors types are always operational, the CDF for ε and ρ is still (19) and (24), but where $\tilde{\mu}$ is substituted for $\tilde{\mu}_t$. Finally, the median for the localization MSE is

$$\text{median}\{\varepsilon(\mathcal{N}_a)\} = \frac{G^{(-1)}(0.5)}{\sum_{t=1}^{T} \frac{\mu_t \alpha_t}{\sigma_t^2}}, \tag{29}$$

and the median for the RMS localization error is

$$\text{median}\{\rho(\mathcal{N}_a)\} = \left(\frac{G^{(-1)}(0.5)}{\sum_{t=1}^{T} \frac{\mu_t \alpha_t}{\sigma_t^2}}\right)^{\frac{1}{2}}. \tag{30}$$

The overall cost of the of the network is the sum the cost of each component of type t

$$\mathcal{C} = \sum_{t=1}^{T} \zeta_t N_t. \tag{31}$$

The goal of the network designer is to determine the best mix of sensors types so that the overall cost is less than or equal to a constraint K. A reasonable design objective is to minimize the median MSE given in (30) given the cost constraint. Dividing both size of (31) by the area A leads to the cost constraint in terms of node density. When all sensors types are always operational, minimization of (30) is equivalent to maximization of its reciprocal so that the objective with the constraints is a linear program

$$\arg \max_{\mu_1, \ldots, \mu_T} \sum_{t=1}^{T} \frac{\mu_t \alpha_t}{\sigma_t^2}, \tag{32}$$

given

$$\begin{aligned} \mu_1 &\geq 0,\\ &\vdots\\ \mu_T &\geq 0,\\ \sum_{t=1}^{T} \zeta_t \mu_t &\leq \frac{K}{A}. \end{aligned} \tag{33}$$

The solution of any linear program lies on one of the vertices of the simplex formed by the constraints [23, Ch. 8.1]. For this linear program, the vertices of the simplex include only one nonzero μ_t. In other words, the optimal network is a homogenous network consisting of sensor type t^* corresponding to the largest conceivable normalized density, i.e., the density that meets the cost constraint,

$$\tilde{\mu}_{t^*} = \max_t \frac{1}{\zeta_t} \frac{K}{A} \frac{\alpha_t}{\sigma_t^2}. \tag{34}$$

When all the sensor types are operational, the solution is simple because the nodes are collecting the same form of information about the targets. One simply chooses the sensor types that provides the most accurate form of this information. Replacing any set of nodes with another type simply degrades the quality of the information. The more interesting case is when some sensor types are not always operational. Then, a cheaper less accurate but more robust node may actually provide utility vis-à-vis the more expensive node. Let o_t be a binary variable that represents whether sensor type t is operational $o_t = 1$ or not $o_t = 0$. Then, for the general case that $p_{\text{op},t} \leq 1$, the CDF for the localization RMS error is

$$\begin{aligned} F_\rho(\rho) = &\sum_{o_1=0}^{o_1=1} \cdots \sum_{o_T=1}^{o_T=1} P(o_1, \ldots, o_T) \cdot & (35)\\ &\cdot G\left(\left(\sum_{t=1}^{T} o_t \frac{\mu_t \alpha_t}{\sigma_t^2}\right) \rho^2\right), \end{aligned}$$

where

$$P(o_1, \ldots, o_T) = \prod_{t=1}^{T} p_{\text{op},t}^{o_t} (1 - p_{\text{op},t})^{(1-o_t)}. \tag{36}$$

The CDF for the localization MSE is obtained by simply substituting ε for ρ^2 in (35), and median statistics for ρ and ε are easily obtained from the CDFs.

The pitfall with the partially operational model that leads to (35) is that is assumes that one sensor modality becomes nonoperational independent of another. In practice, designers choose node modalities to complement each other. In other words, when conditions are poor for one modality, they should be OK for another one. A better model is that the operational probability of nodes types are correlated. This will be a subject of future work. The simulations focus on the specific case of the analog of acoustic array and camera nodes whose first order models are described in Section 2.

Let $t = 1$ and $t = 2$ correspond to the acoustic and camera nodes, respectively. Then, the localization RMS error CDF in (35) simplifies to

$$F_\rho(\rho) = p_{\text{op},2} G\left(\left(\frac{\mu_1\alpha_1}{\sigma_1^2} + \frac{\mu_2\alpha_2}{\sigma_2^2}\right)\rho^2\right) + (1 - p_{\text{op},2}) G\left(\left(\frac{\mu_1\alpha_1}{\sigma_1^2}\right)\rho^2\right). \quad (37)$$

The median RMS localization error is the ρ^* that solves

$$p_{\text{op},2} G\left(\left(\frac{\mu_1\alpha_1}{\sigma_1^2} + \frac{\mu_2\alpha_2}{\sigma_2^2}\right)\rho^{*2}\right) + (1 - p_{\text{op},2}) G\left(\left(\frac{\mu_1\alpha_1}{\sigma_1^2}\right)\rho^{*2}\right) = \tfrac{1}{2}. \quad (38)$$

Again, the designer can search for the densities μ_t for $t = 1, 2$ that minimize ρ^2 under the constraints for cost and positive densities (see (33)). Unlike the simple case that $p_{\text{op},t} = 1$, the minimization problem is not a linear program. For two sensor modalities, there is one degree of freedom, i.e., μ_1 or μ_2. In the simulations, we illustrate how the median RMS localization error changes over this degree of freedom.

5. SIMULATIONS

In this section, we confirm the design characterization presented in Section 4 against Monte carlo simulations. The first set of simulations generate random configurations of the nodes by uniformly distributing them over a circular region of radius 1.6km. Furthermore, the orientation of the cameras are uniformly distributed over $[0, 2\pi)$. An example of such a random configuration for 100 acoustic arrays ($\mu_1 = 12.5$ nodes/km^2) and 10 cameras ($\mu_2 = 1.25$ nodes/km^2) is shown in Figure 2. The "$\circ$" and "$\vee$" symbols represent the acoustic and camera nodes, respectively. The target is located at the center of the region. When the target is within the FOV of the camera, a small cross-bar is added to the "$\vee$" symbol to form a "$\forall$" symbol. This cross-bar represents the lens of the camera. Therefore, one can infer which camera nodes have line-of-sight to the target based on their orientation. The figure also shows the nodes selected by the "normalized closest" management method as the brighter color symbols.

We consider the case where a budget of 1200 monetary units is available to build a sensor network to cover the circular region of radius 1.6 km. Therefore, one could design a homogenous network of 1200 acoustic nodes with density $\mu = 150$ nodes/km^2 or 120 camera nodes with density

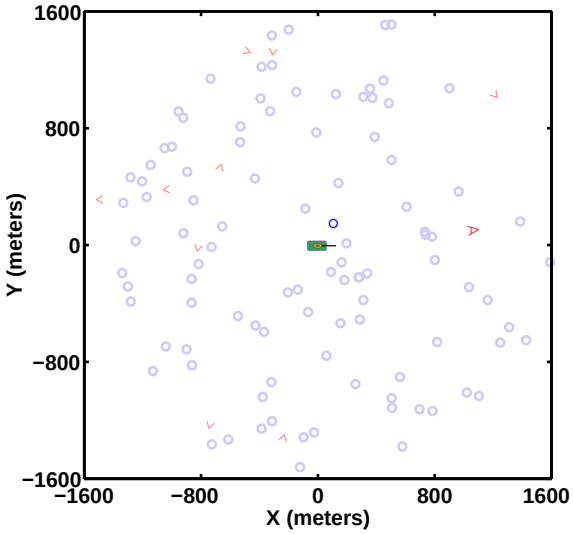

Figure 2. Example of random sensor configuration of 100 acoustic arrays ($\circ$) and 10 cameras ($\vee$) with the target located in the center. One camera ($\forall$) has line-of-sight to the target. The brighter colored nodes represent the selected nodes.

$\mu = 15$ nodes/km^2. Alternatively, one could design a heterogeneous network where the acoustic and camera densities are $\mu_1 = 150 - 10y$ and $\mu_2 = y$, respectively, for $0 < y < 15$. The normalized FOV of the cameras is $\alpha_2 = \frac{1}{12}$. Given the design characterization presented in Section 4 and the models provided in Section 2, the theoretical RMS localization error for "normalized closest" node selection is computed using (38). This formula is valid for any point well inside the support of the network. To verify the theory, we generated 10,000 random configurations for each value of the degree of freedom y and $p_{\text{op},2}$. Then, we sorted the normalized distances squared to the a center of the region and employed (10) and (13) to determine the instantaneous RMS localization error. Finally, we calculated the median error over all 10,000 configurations. Figure 3 provides the results of both the theory and the Monte Carlo simulations.

Figure 3(a) provides the localization error versus node density curves for various values of $p_{\text{op},2}$. The figure shows very good agreement between the theory and the simulations. When $p_{\text{op},2} = 1$, the error curve is monotonically decreasing as the error camera density increases. The design characterization in Section 4 indicates that this curve must be monotonic (either decreasing or increasing) because a heterogeneous network can not lead to minimum error. For our models, it turns out that the best design choice when the cameras can always make measurements is to deploy the 120 cameras that are within budget. The $p_{\text{op},2} = 1$ case also represents the achievable performance conditioned on the fact that the cameras are operational. On the other hand, when $p_{\text{op},2} = 0$, the error curve is monotonically increasing because as the camera density increases, the cameras are providing no assistance for localization. As a result, the density of the useful acoustic nodes is simply decreasing and performance is degrading

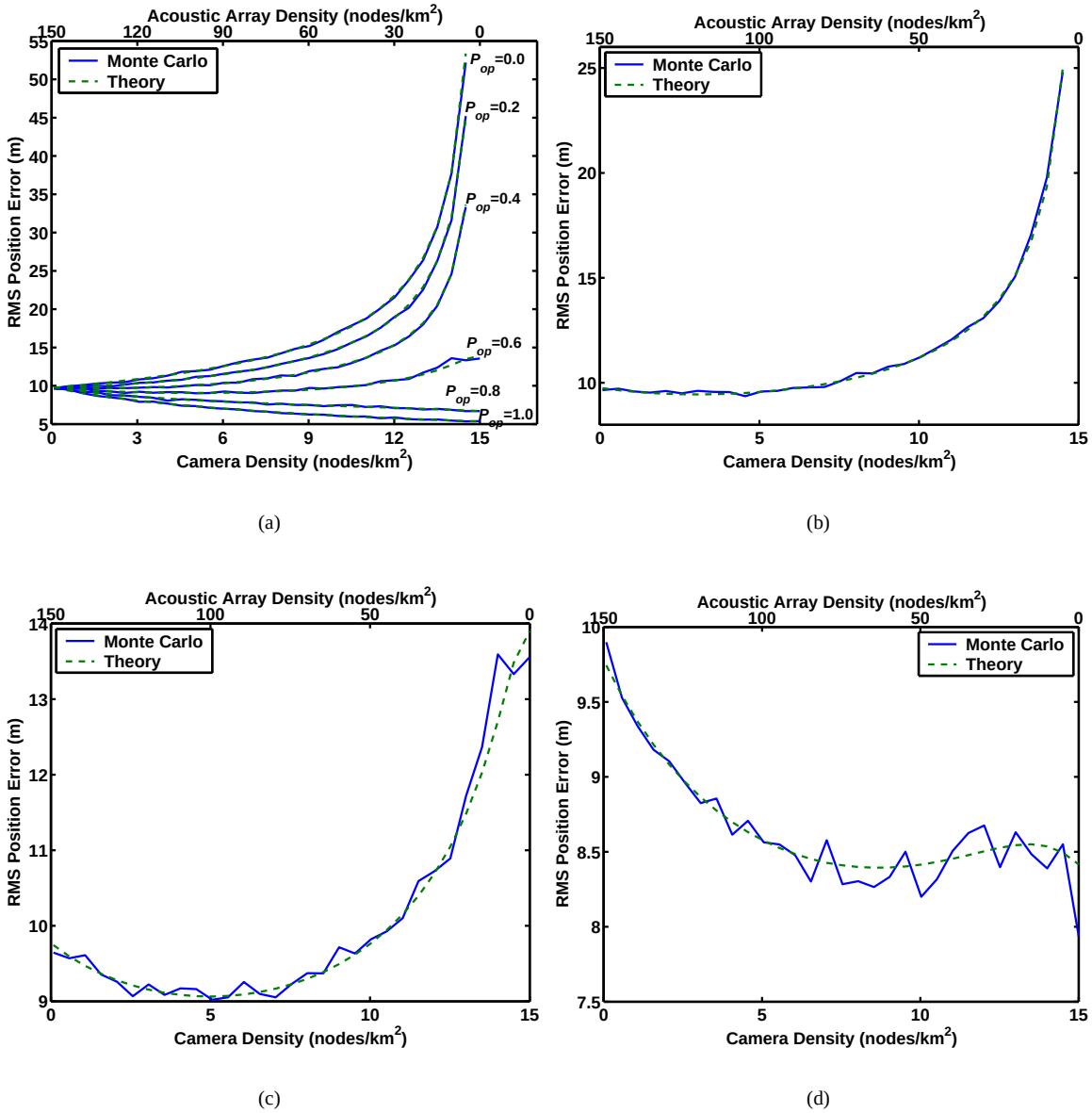

Figure 3. Median RMS localization error as a function of admissible number of camera and acoustic nodes under different conditions for the operational probability of the cameras: (a) Various $p_{\text{op},2}$, (b) $p_{\text{op},2} = 0.5$, (c) $p_{\text{op},2} = 0.6$, and (d) $p_{\text{op},2} = 0.7$.

(see (26)), and when $\mu_1 = 0$, then the median value diverges to infinity because no sensors are available to localize the target. Clearly, if the cameras are not useful, the best design is to deploy the 1200 acoustic arrays that are within budget. The $p_{\text{op},2} = 0$ curve also represents the worst case performance, i.e., when the cameras are unable to make useful measurements.

The design decisions become more interesting when $0 < p_{\text{op},2} < 1$. It can be shown that when $0 < p_{\text{op},2} \leq 0.5$, then the median RMS localization error diverges to infinity as μ_1 goes to zero. Once $p_{\text{op},2}$ exceeds 0.5, the median error is finite as μ_1 goes to zero, and as $p_{\text{op},2}$ goes to one, the median localization error at $\mu_1 = 0$ is decreasing with respect to $p_{\text{op},2}$. For the given sensor parameters, it turns out that the median error for $\mu_1 = 150$ (or $\mu_2 = 0$) is less than the median error for $\mu_1 = 0$ (or $\mu_2 = 15$) as long as $p_{\text{op},2} < 0.66$. In other words, the error curve has a higher value at $\mu_1 = 0$ than it does when $\mu_1 = 150$. When $p_{\text{op},2} > 0.66$, the median error for $\mu_1 = 150$ is greater than the error for $\mu_1 = 0$. As discussed in the previous paragraph, the error curves in Figure 3(a) must be monotonic for $p_{\text{op},2} = 0$ or $p_{\text{op},2} = 1$. However, one can see in the figure that error curves are not monotonic as long as the operational probability is within two thresholds $0 < \underline{\tau} \leq p_{\text{op},2} \leq \overline{\tau} < 1$.

Figures 3(b), (c), (d) provide the specific error curves for the cases that $p_{\text{op},2} = 0.5$, $p_{\text{op},2} = 0.6$, and $p_{\text{op},2} = 0.7$, re-

Table 1. Nearly optimal design ranges that meet the 1200 monetary unit budget for various values of $p_{\text{op},2}$.

$p_{\text{op},2}$	Acoustic Arrays	Cameras
0.5	$N_1: \quad 1200 \leftrightarrow 680$	$N_2: \quad 0 \leftrightarrow 52$
	$\mu_1: \quad 150 \leftrightarrow 85$	$\mu_2: \quad 0 \leftrightarrow 6.5$
0.6	$N_1: \quad 1100 \leftrightarrow 510$	$N_2: \quad 10 \leftrightarrow 69$
	$\mu_1: \quad 138 \leftrightarrow 64$	$\mu_2: \quad 1.3 \leftrightarrow 8.6$
0.7	$N_1: \quad 780 \leftrightarrow 130$	$N_2: \quad 42 \leftrightarrow 107$
	$\mu_1: \quad 98 \leftrightarrow 16$	$\mu_2: \quad 5.3 \leftrightarrow 13.4$

spectively. The vertical axes for these figures accentuate the dynamic range of these specific curves as compared to Figure 3(a). All three curves have a minimum that corresponds to a heterogeneous network solution. Fortunately, the minimum is not very "sharp" so that nearly optimal performance is achievable over a range of densities. For instance, the reasonable ranges for the design parameters are provided in Table 1 for these three values of $p_{\text{op},2}$. The curves in Figures 3(b)-(d) represent the typical performance of the network taking into account the times when the cameras are providing and not providing data. For the specific times that the cameras are (or are not) collecting data, then the $p_{\text{op},2} = 1$ (or $p_{\text{op},2} = 0$) curve in Figure 3(a) represents the typical performance.

The simulations that generated Figure 3 did not actually run any localization technique. They simply computed (13) based upon the geometry of the realization of the random network configuration. Furthermore, these simulations always placed the target at the center of the deployment region. The next set of simulations consider the case of a moving target traveling at constant velocity of magnitude 10 m/s through a rectangular deployment region of size 1km $\times$ 2km. The initial location of the target is determined by the standard nonlinear least squared method described in [13], [17] that represents the maximum likelihood estimator for the AWGN model given by (1) when $\phi^* = \phi$ for each node [17]. Then, a bearings-only EKF tracker continues to estimate the target position at each snapshot time. At each snapshot of the tracking, the "normalized closest" method selects the two nodes collect the measurement to be fed into the EKF tracker. The EKF employs the discrete white noise acceleration model with process noise $\sigma_\upsilon = 5$ m/s^2 [24]. The specific details about the bearing-only EKF tracker can be found in [3].

Figure 4 illustrates how the tracking of the target and selection of nodes at various snapshots of time for a heterogeneous network. This particular network consists of 50 acoustic ($\circ$) and 10 camera ($\vee$) nodes. The FOV of the cameras is $\alpha_2 = \frac{1}{12}$ (30°). Again, when the target is within the FOV of the camera, a cross-bar is added to the "$\vee$" symbol to form the "$\forall$" symbol to represent the camera. The target is moving from the left to the right. The graphs in the figure indicate the state of the nodes for various collection snapshots of time. Overall, the EKF is tracking target for 100 snapshots. When the camera can see the target, it is colored in a bright red; otherwise, it is colored in a dull red. When a node is selected for a given snapshot, a dotted line protrudes from the node to the estimated target location. The graphs in the figure indicate that the EKF is effectively estimating the target location at each point in time. Whenever, a camera can see the target, the camera is chosen because the bearing RMS error is so small much smaller for the cameras (0.25° versus 5°).

For the next set of simulations, the budget is 300 monetary units so that an admissible network design will contain $N_1 = 300 - 10y$ acoustic nodes ($\mu_1 = 150 - 5y$ nodes/km^2) and $N_2 = y$ camera nodes ($\mu_2 = \frac{1}{2}y$ nodes/km^2) for $0 \leq y \leq 30$ over the 2 km^2 region. The probability that the cameras collect useful information is set to $p_{\text{op},2} = 0.6$. First, we first consider the case that the camera have a wide field of view $\alpha_2 = \frac{1}{3}$ (120°). For each value of the degree of freedom y, fifty random network configurations were generated, and the EKF tracks the target over 100 Monte Carlo realization for a given network configuration. Each track provides 100 estimated target positions for a total 10,000 RMS localization error values per configuration, or 500,000 values per a design posibility y. Figure 5(a) plots the median RMS localization error versus the admissible node densities. The figure also includes the median error predicted via (38). The two curves have the same shape, but they do not overlap because they represent slightly different quantities. Specifically, the theory represents the "median" over all possible node/target geometries of the "average" error for a particular node/target geometry. On the other hand, the simulations provide a median over geometries and random realization for that geometry. Figure 5(b) shows the same plots of the same two curves except that a constant factor of 2.3 m is added to the simulated results. Remarkably, the two curves agree in shape and in dynamic range. The suggestion by theory to choose $N_1 = 140$ acoustic nodes ($\mu_1 = 70$ nodes/km^2) and $N_2 = 16$ camera nodes ($\mu_2 = 8$ nodes/km^2) is confirmed to be reasonable by the simulations.

The next set of simulations considers cameras with narrower FOVs. Specifically, the FOV of the cameras is $\alpha_1 = \frac{1}{12}$ (30°). Again, the median RMS localization error is computed over 100 Monte Carlo runs of an EKF tracker for each of 50 different random configurations. Figure 6 provides the resulting localization error versus node density curves. This time, the theory did not match the simulations as well as it did for the wider FOV camera. The simulated error grows too quickly for the larger camera densities. The reason for the discrepancy is due to the limited number of camera nodes relative to the FOV inside the finite deployment region. The theory assumes an infinite deployment region. For any value of $0 < y \leq 30$, there is a high probability that a camera node does not see the target. The theory assumes that there is always a node that sees the target. The expected distance of the node to the target is simply pushed out as the FOV becomes narrower. It can be the case that the normalized distances $\tilde{r}_i$ for $i = 1, 2$ of the narrow FOV camera nodes are still exceeded by those of the acoustic nodes even though there is

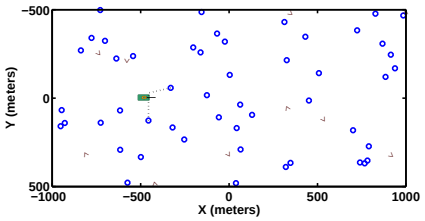

(a)

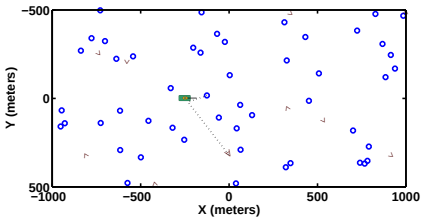

(b)

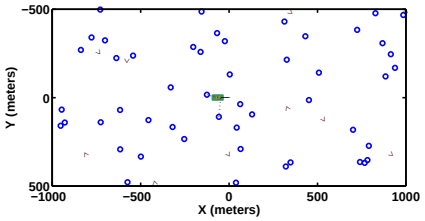

(c)

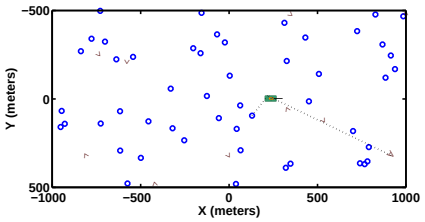

(d)

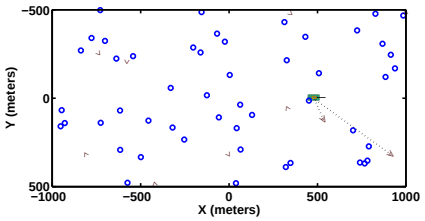

(e)

Figure 4. Illustration of sensor selection and localization for a heterogeneous network of 50 acoustic ($\circ$) and 10 camera ($\vee$) nodes during EKF tracking. Cameras with line-of-sight to the target are represented by the "$\forall$" symbol.

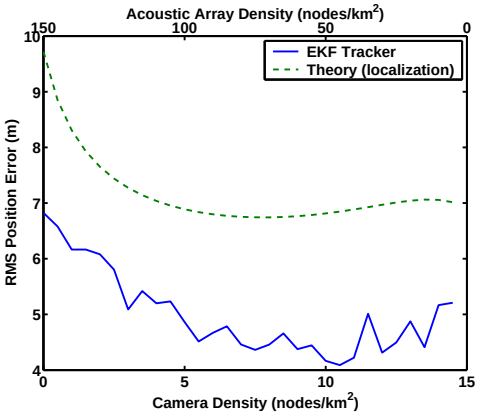

(a)

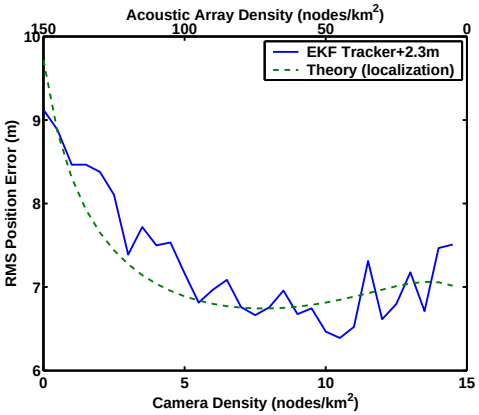

(b)

Figure 5. Median RMS localization error over EKF tracking as a function of admissible number of camera and acoustic nodes when the cameras' normalized FOV is $\alpha_2 = \frac{1}{3}$ and the deployment region is 1km $\times$ 2km: (a) Simulation and theoretical results, and (b) median shifted simulated and theoretical results.

a high probability that the actual distances r_i for the camera nodes exceed the dimensions of the finite region. This is case in Figure 6, and when the camera density increases, the theory becomes too optimistic.

We reran the simulations of the narrow FOV cameras for a larger deployment region. For these simulations, the region is now 2km $\times$ 4km, and the budget has increased to 1200 monetary units. The admissible network design now contains $N_1 = 1200 - 10y$ acoustic nodes ($\mu_1 = 150 - 5y$ nodes/km^2) and $N_2 = y$ camera nodes ($\mu_2 = \frac{1}{8}y$ nodes/km^2) for $0 \leq y \leq 120$ over the 8 km^2 region. The range of admissible densities is exactly the same as in Figure 6. Figure 7(a) plots the median RMS localization error versus node density for both simulated and theoretical results. Figure 7(b) plots the same two curves except that a constant value of 3 m is

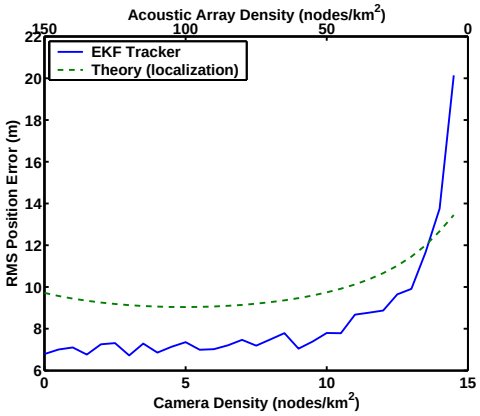

Figure 6. Median RMS localization error over EKF tracking as a function of admissible number of camera and acoustic nodes when the cameras' normalized FOV is $\alpha_2 = \frac{1}{12}$ and the deployment region is 1km $\times$ 2km.

added to the simulated results. Clearly, the shape and dynamic range of the two curves are in agreement. The deployment region of areas 8 km^2 is large enough to avoid the finite effects of a camera FOV of 30°. Finally, the simulations confirm that the design of $N_1 = 810$ acoustic nodes ($\mu_1 = 101$ nodes/km^2) and $N_2 = 39$ camera nodes ($\mu_t = 4.9$ nodes/km^2) is reasonable.

6. CONCLUSIONS

This paper presents a first order theory to determine typical localization errors when a heterogeneous network of bearings-only nodes are localizing a target using a sensor management strategy to conserve node usage, i.e., energy. The "normalized closest" sensor management approach is considered in order for the analysis to be tractable. The mean error actually diverges because of the high probability that the closest approach provides a poor geometry. Therefore, the median error is used as the typical value. This theory can be used to determine the best mix of sensor types under a cost constraint. If all the senor types are always able to collect measurements, it is best to select the homogeneous network of highest admissible density (within cost) that provides the lowest typical error. This result is intuitive since all sensors types are collecting the same type measurements about the target, i.e., geolocation measurements. However, when a particular sensor modality is unable to provide measurements under all environmental conditions, a heterogeneous network can become desirable. The paper provides examples when a heterogeneous network that meets the cost constraints actually provides the lowest median localization error. Finally, simulations confirm that the theory is valid as long as critical mass of nodes of any modality can see the target at a given snapshot.

While the theory is a good first step towards providing design guidance for a heterogeneous network, it is not the final answer. The theory should be expanded to account for the ef-

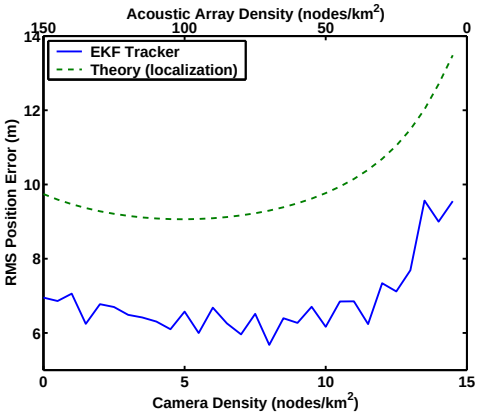

(a)

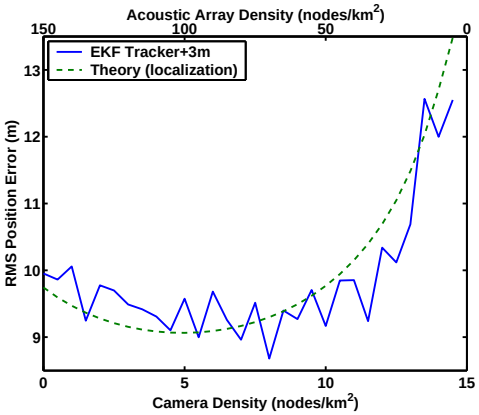

(b)

Figure 7. Median RMS localization error over EKF tracking as a function of admissible number of camera and acoustic nodes when the cameras' normalized FOV is $\alpha_2 = \frac{1}{12}$ and the deployment region is 2km $\times$ 4km: (a) Simulation and theoretical results, and (b) median shifted simulated and theoretical results.

fects of the finite size of the deployment region, and consider the coupling between the environment and the usefulness of measurements from various sensor modalities, i.e., the correlations between p_{op_t}. Currently, the design goal only considers geolocation performance. In the future, additional design goals such as the communication cost and classification accuracy should be considered. For instance, it is desirable for the aggregate node density to be high for a low transmission range, and that the number of hops between active nodes to be low. In addition, the theory must eventually take into account the detection probability of nodes, which is a function of range to the target. In fact, detection alone can be used for localization [25] and the performance of such approaches have been characterized in [26], [27]. The determination of the best mixture of nodes in a senor network is a multi-faceted problem that will keep the research community engaged for

years to come.

APPENDIX

1. DERIVATION OF LOCALIZATION ERROR STATISTICS

This appendix derives the statistics for the localization error when employing the "normalized closest" sensor management approach in a homogeneous network of normalized density $\tilde{\mu}_t$. The localization error is a function of $\tilde{r}_i$ and ϕ_i for $i = 1, 2$ as given by (13). The numerator in (13) can be rewritten in terms of the normalized squared distances as

$$\tilde{r}_1^2 + \tilde{r}_2^2 = \tilde{s}_1 + \tilde{s}_2. \tag{39}$$

Then, the joint PDF of the random variables that affect the value of ε is

$$f(\tilde{s}_1, \tilde{s}_2, \phi_1, \phi_2) = \left(\frac{\tilde{\mu}_t}{2}\right)^2 e^{-\pi\tilde{\mu}_t\tilde{s}_2} \tag{40}$$

for $0 \leq \tilde{s}_1 \leq \tilde{s}_2$ and $0 \leq \phi_1, \phi_2 < 2\pi$. The polar angles are statistically independent of the normalized distances squared. Therefore, the joint PDF can be expressed as the product of two marginal distributions,

$$f(\tilde{s}_1, \tilde{s}_2) = (\pi\tilde{\mu}_t)^2 e^{-\pi\tilde{\mu}_t\tilde{s}_2} \tag{41}$$

for $0 \leq \tilde{s}_1 \leq \tilde{s}_2$ and

$$f(\phi_1, \phi_2) = \frac{1}{(2\pi)^2} \tag{42}$$

for $0 \leq \phi_1, \phi_2 < 2\pi$.

Let's determine the distribution for numerator and denominator of (13). The denominator is a nonlinear function of the modulo 2π difference of two independent random variables ϕ_1 and ϕ_2 with uniform distributions. It is well known that the modulo 2π difference,

$$\phi_\Delta = \phi_1 - \phi_2, \tag{43}$$

is also uniformly distributed over $[0, 2\pi)$. Now, the denominator is

$$b = \sin^2\phi_\Delta, \tag{44}$$

and it can be shown that the distribution for b is

$$f(b) = \frac{1}{\pi}\frac{1}{\sqrt{b}\sqrt{1-b}}, \tag{45}$$

for $0 \leq b \leq 1$.

The distribution for the numerator is determined by considering the following changes of variables,

$$\begin{aligned} s &= \tilde{s}_1 + \tilde{s}_2, \\ w &= -\tilde{s}_1 + \tilde{s}_2. \end{aligned} \tag{46}$$

Since the joint PDF for $\tilde{s}_1$ and $\tilde{s}_2$ is given by (41), the joint PDF for s and w is

$$f(s, w) = \frac{(\pi\tilde{\mu}_t)^2}{2} e^{-pi\tilde{\mu}_t\frac{s+w}{2}} \tag{47}$$

for $s \geq w \geq 0$. Then, by integrating out w, the marginal distribution for the numerator s is

$$f(s) = \pi\tilde{\mu}_t\left(e^{-\frac{\pi\tilde{\mu}_t s}{2}} - e^{-\pi\tilde{\mu}_t s}\right) \tag{48}$$

for $s \geq 0$.

Now, the expected value of ε is

$$\begin{aligned} E\{\varepsilon\} &= \int_0^\infty\int_0^1 \frac{s}{b} f(s)f(b)dsdb, & (49)\\ &= \int_0^\infty sf(s)ds \int_0^1 \frac{1}{b} f(b)db. & (50) \end{aligned}$$

After a little work, it can be shown that

$$\int_0^\infty sf(s)ds = \frac{3}{\pi\tilde{\mu}_t}. \tag{51}$$

However, the expected value of the reciprocal of the denominator has problems,

$$\int_0^1 \frac{1}{b} f(b)db = \int_0^1 \frac{1}{\pi}\frac{1}{b\sqrt{b}\sqrt{1-b}}db. \tag{52}$$

Using the change of variable $c = \frac{1}{b} - 1$, the integral is equal to

$$\int_0^\infty \frac{1}{\pi}\frac{1}{\sqrt{c}}dc = \lim_{c\to\infty}\frac{2}{\pi}\sqrt{c}, \tag{53}$$

which diverges to infinity. Therefore, the localization MSE given in (13) does not have a finite expected value. Similar arguments can show that the localization RMS error ρ, i.e., the square root of the MSE, also does not have a finite mean. The divergence of the mean for $\frac{1}{b}$ or $\frac{1}{\sqrt{b}}$ is due to the high probability that $b = 0$ or equivalently $\phi_\Delta = 0$. When $\phi_\Delta = 0$, the two nodes and the target are collinear, which is the degenerate geometry for triangulation.

Even though ε does not have a finite mean, we can still derive its CDF,

$$\begin{aligned} F_\varepsilon(x) &= \text{Prob}(\epsilon \leq x), & (54)\\ &= \text{Prob}(\frac{s}{b} \leq x), & (55)\\ &= \text{Prob}(s \leq bx), & (56)\\ &= \int_0^1\int_0^{bx} f(s)f(b)dsdb, & (57)\\ &= \int_0^1 (1 - 2e^{-\frac{\pi\tilde{\mu}_t}{s}bx} + e^{\pi\tilde{\mu}_t bx})f(b)db. & (58) \end{aligned}$$

Using the change of variable $b = \sin\theta$, the CDF can be reexpressed as

$$F_\varepsilon(x) = 1 - 2\beta\left(\frac{\tilde{\mu}_t}{2}x\right) + \beta(\tilde{\mu}_t x), \tag{59}$$

where

$$\beta(x) = \frac{1}{\pi}\int_0^\infty e^{-\pi x \sin^2\theta} d\theta. \quad (60)$$

It is convenient to consider the CDF for the special case that $\tilde{\mu}_t = 1$,

$$G(x) = 1 - 2\beta\left(\frac{1}{2}x\right) + \beta(x). \quad (61)$$

Then, the CDF for ε associated to arbitrary density $\tilde{\mu}_t$ is a dilation of G,

$$F_\varepsilon(x) = G(\tilde{\mu}_t x). \quad (62)$$

The median value of ε corresponds to the point where the CDF equals 0.5. Therefore,

$$\begin{aligned} F_\varepsilon(\text{median}\{\varepsilon\}) &= 0.5, & (63)\\ G(\tilde{\mu}_t \text{median}\{\varepsilon\}) &= 0.5, & (64)\\ \text{median}\{\varepsilon\} &= \frac{G^{(-1)}(0.5)}{\tilde{\mu}_t}. & (65)\end{aligned}$$

Numerical computation shows that $G^{(-1)}(0.5) \approx 1.86$. Thus,

$$\text{median}\{\varepsilon\} \approx \frac{1.86}{\tilde{\mu}_t}. \quad (66)$$

The CDF for the localization RMS error ρ is easy to derive from the CDF of ε,

$$\begin{aligned} F_\rho(x) &= \text{Prob}(\rho \le x), & (67)\\ &= \text{Prob}(\varepsilon \le x^2), & (68)\\ &= F_\varepsilon(x^2), & (69)\\ &= G(\tilde{\mu}_t x^2). & (70)\end{aligned}$$

Finally, the median of ρ is

$$\begin{aligned} \text{median}\{\rho\} &= \left(\frac{G^{(-1)}(0.5)}{\tilde{\mu}_t}\right)^{\frac{1}{2}}, & (71)\\ &\approx \frac{1.3639}{\sqrt{\tilde{\mu}_t}}. & (72)\end{aligned}$$

REFERENCES

[1] D. Estrin, L. Girod, G. Pottie, and M. Srivastava, "Instrumenting the world with wireless sensor networks," in *Proc. of IEEE ICASSP 2001*, vol. 4, pp. 2033–2036, May 2001.

[2] V. Raghunathan, C. Schurgers, S. Park, and M. Srivastava, "Energy-aware wireless microsensor networks," *IEEE Signal Processing Magazine*, vol. 19, pp. 40–50, Mar. 2002.

[3] L. M. Kaplan, "Global node selection for localization in a distributed network," *IEEE Trans. on Aerospace and Electronic Systems*, pp. 136–146, Jan. 2006.

[4] L. M. Kaplan, "Local node selection for localization in a distributed network," *IEEE Trans. on Aerospace and Electronic Systems*, pp. 113–135, Jan. 2006.

[5] R. A. Burne, I. Kadar, and A. Buczak, "A self-organizing, cooperative sensor network for remote surveillance: Target tracking while optimizing the geometry between bearing-reporting sensors and the target," in *Proc. of SPIE*, vol. 4393, Apr. 2001.

[6] F. Zhao, J. Shin, and J. Reich, "Information-driven dynamic sensor collaboration," *IEEE Signal Processing Magazine*, vol. 19, pp. 61–72, Mar. 2002.

[7] M. Chu, H. Haussecker, and F. Zhao, "Scalable information-driven sensor querying and routing for ad hoc heterogeneous sensor networks," *International Journal of High Performance Computing Applications*, vol. 16, Aug. 2002.

[8] J. Liu, J. Reich, and F. Zhao, "Collaborative in-network processing for target tracking," *EURASIP Journal on Applied Signal Processing*, vol. 2003, pp. 378–391, Mar. 2003.

[9] V. Cevher, L. M. Kaplan, U. Sung, and L. Clare, "A Bayesian acoustic sensor network build strategy for position tracking." in preparation for *IEEE Transactions on Signal Processing*.

[10] V. Isler and R. Bajcsy, "The sensor selection problem for bounded uncertainty sensing models," in *Fourth Intl. Symp. on Information Processing in Sensor Networks (IPSN)*, pp. 151–158, Apr. 2005.

[11] I. Kadar, "Optimum geometry selection for sensor fusion," in *Proc. of SPIE*, vol. 3374, pp. 96–107, Apr. 1998.

[12] J. M. Manyika and H. F. Durrant-Whyte, *Data Fusion and Sensor Management: An Information-Theoretic Approach*. Englewood Cliffs, NJ: Prentice Hall, 1994.

[13] L. M. Kaplan and Q. Le, "On exploiting propagation delays for passive target localization using bearings-only measurements," *Journal of Franklin Institute*, vol. 342, pp. 193–211, Mar. 2005.

[14] D. K. Wilson, B. M. Sandler, and T. Pham, "Simulation of detection and beamforming with acousitcal ground sensors," in *Proc. of SPIE*, vol. 4743, pp. 50–61, 2002.

[15] S. Chandran, ed., *Advances in Direction-of-Arrival Estimation*. Norwood, MA: Artech House, 2006.

[16] J. M. Mendel, *Lessons in Digital Estimation Theory*. Englewood Cliffs, NJ: Prentice Hall, 1987.

[17] Y. Oshman and P. Davidson, "Optimization of observer trajectories for bearings-only target localization," *IEEE Trans. on Aerospace and Electronic Systems*, vol. 35, pp. 892–902, July 1999.

[18] L. M. Kalan, Q. Le, and P. Molnar, "Maximum likelihood methods for bearings-only target localization," in *Proc. of the IEEE International Conference on Acoustics, Speech, and Signal Processing (ICASSP)*, vol. 5, pp. 3001–3004, May 2001.

[19] A. Farina, "Target tracking with bearing-only measure-

ments," *Signal Processing*, vol. 78, pp. 61–78, Jan. 1999.

[20] R. G. Stransfield, "Statistical theory of D.F. fixing," *IEE (London)*, vol. 94, pp. 762–770, 1947.

[21] S. M. Ross, *Introduction to Probability Models*. San Diego, CA: Academic Press, eighth ed., 2003.

[22] R. Mathar and J. Mattfeldt, "On the distribution of cumulated interference power in Rayleigh fading channels," *Wireless Networks*, vol. 1, pp. 31–36, Feb. 1995.

[23] G. Strang, *Introduction to Applied Mathematics*. Wellesley, MA: Wellesley-Cambridge Press, 1986.

[24] Y. Bar-Shalom, X. R. Li, and T. Kirubarajan, *Estimation with Application to Tracking and Navigation*. New York: John Wiley & Sons, 2001.

[25] A. Artes-Rodriguez, M. Lazaro, and L. Tong, "Target location estimation in sensor networks using range information," in *Proc. of the 2004 IEEE Sensor Array and Multichannel Signal Processing Workshop*, pp. 608–612, July 2004.

[26] A. Capponi, C. Pilotto, G. Golino, A. Farina, and L. Kaplan, "Algorithms for the selection of the active sensors in distributed tracking: Comparison between Frisbee and GNS methods," in *Proc. of the International Conference on Information Fusion*, (Florence, Italy), July 2006.

[27] A. Capponi, L. Kaplan, and C. Pilotto, "Performance characterization of random proximity sensor networks," in *Proc. of the Asilomar Conference on Signals, Systems, and Computers*, 2006.

Lance M. Kaplan *(S'88 M'89 SM'00) received the B.S. degree with distinction from Duke University, Durham, NC, in 1989 and the M.S. and Ph.D. degrees from the University of Southern California, Los Angeles, in 1991 and 1994, respectively, all in Electrical Engineering. From 1987-1990, Dr. Kaplan worked as a Technical Assistant at the Georgia Tech Research Institute. He held a National Science Foundation Graduate Fellowship and a USC Deans Merit Fellowship from 1990-1993, and worked as a Research Assistant in the Signal and Image Processing Institute at the University of Southern California from 1993-1994. Then, he worked on staff in the Reconnaissance Systems Department of the Hughes Aircraft Company from 1994-1996. From 1996-2004, he was a member of the faculty in the Department of Engineering and a senior investigator in the Center of Theoretical Studies of Physical Systems (CTSPS) at Clark Atlanta University (CAU), Atlanta, GA. Currently, he is a team leader in the EO/IR Image Processing branch of the U.S. Army Research Laboratory. Dr. Kaplan serves as Associate Editor-In-Chief and EO/IR Systems Editor for the IEEE Transactions on Aerospace and Electronic Systems. He is also a three time recipient of the Clark Atlanta University Electrical Engineering Instructional Excellence Award from 1999-2001. His current research interests include signal and image processing, automatic target recognition, data fusion, and resource management.*

Volkan Cevher *was born in Ankara, Turkey, in 1978. He received his B.S. degree in Electrical Engineering from Bilkent University, Ankara, Turkey in 1999 as a valedictorian. During summer of 2003, he was employed by Schlumberger Doll Research. In Fall 2004, he was the co-recipient of the Center for Signal and Image Processing Outstanding Research Award. He received his Ph.D. degree in Electrical Engineering from Georgia Institute of Technology in 2005. He worked a postdoc at Georgia Institute of Technology under the supervision of Dr. James H. McClellan till the end of 2005. He is currently working with Dr. Rama Chellappa as a research associate on computer vision problems. His research interests include structure from motion, sensor network management problems (sensor build and placement strategies), Monte-Carlo Markov chain methods (specifically particle filters), target tracking models, adaptive filters, time frequency distributions, fractional Fourier transform, brain-computer interface problems, and array signal processing.*